Available online at www.sciencedirect.com
ScienceDirect
Remote Sensing of Environment 105 (2006) 221–236
Remote Sensing of Environment
www.elsevier.com/locate/rse

A satellite-derived climatology of global ocean winds

Craig M. Risien *, Dudley B. Chelton

College of Oceanic and Atmospheric Sciences, 104 COAS Administration Building, Oregon State University, Corvallis, OR 97331-5503, United States
Cooperative Institute for Oceanographic Satellite Studies, 104 COAS Administration Building, Oregon State University, Corvallis, OR 97331-5503, United States

Received 17 April 2006; received in revised form 26 June 2006; accepted 28 June 2006

Abstract

An interactive Climatology of Global Ocean Winds (COGOW) is presented based on 5 years (August 1999–July 2004) of QuikSCAT satellite measurements of wind speed and direction 10 m above the sea surface. This climatology provides the first high spatial resolution, observationally based, online atlas of ocean winds. Users can retrieve climatological wind maps and wind statistics, both in tabular and graphical form, from the COGOW web-based atlas. The global coverage of these data provides highly accurate information about the wind statistics in regions of the world ocean that are sparsely sampled by ships and buoys. A case study of the recovery of the vessel *Ehime Maru* off the Hawaiian Island of Oahu is presented to demonstrate the usage and value of COGOW. Evidence of air–sea interactions, one of many wind phenomena visible within COGOW, is discussed to further familiarize users with COGOW. Finally, the utility of COGOW with regard to various operational and research communities is summarized.

Keywords: Climatology; Global ocean winds; QuikSCAT scatterometer

1. Introduction

Knowledge of local, regional and global wind regimes is vital to a number of operational communities. These include oil spill responders, Coast Guard search and rescue teams, state and federal emergency response planning programs, oil and gas companies, marine resource managers, and the international shipping community. An understanding of the global wind field is therefore clearly desirable. Observationally based understanding has long been limited by poor in situ coverage by buoys and ships (Fig. 1a). Even in areas where such observations exist, their distribution is highly variable in both time and space (Fig. 1b and c) and, as such, the in situ data do not adequately resolve global ocean winds. The Fig. 2 reveals that, for the 38-year period January 1960–December 1997, about 70% of grid cells within the Comprehensive Ocean–Atmosphere Data Set (COADS) Release 1 (Slutz et al., 1985; Woodruff et al., 1987) have a total number of wind observations that is less than 900. In other words, about 70% of grid cells in this "global" dataset are sampled on average less than twice per month. The locations of all of the grid cells that have an average sampling rate that equals or exceeds twice per month are shown in Fig. 1b. The locations of all of the grid cells that have an average sampling rate that equals or exceeds once per 3 days are shown in Fig. 1c.

It is clear from Figs. 1 and 2 that wind forcing over vast portions of the global oceans is significantly under-sampled, both temporally and spatially, from ship-based observations. Since July 1999 this situation has changed. Through high-resolution spatial sampling and frequent temporal sampling by the National Aeronautics and Space Agency's (NASA) Quick Scatterometer (QuikSCAT) satellite launched in June 1999, wind speed and direction are sampled daily at a 25 km resolution over approximately 90% of the global oceans. The objective of this study is to use the first 5 years of the QuikSCAT data set to develop an online Climatology of Global Ocean Winds (COGOW).

Two previously published atlases of observationally based global ocean climatological winds are the Marine Climatic Atlas (MCA) (National Climatic Data Center, 2004) and the Atlas of Surface Marine Data 1994 (ASMD94) (Da Silva et al., 1994). The MCA atlas presents monthly climatological data on either a

* Corresponding author. College of Oceanic and Atmospheric Sciences, 104 COAS Administration Building, Oregon State University, Corvallis, OR 97331-5503, United States. Tel.: +1 541 737 4487; fax: +1 541 737 2064.
E-mail address: crisien@coas.oregonstate.edu (C.M. Risien).

0034-4257/$ - see front matter © 2006 Elsevier Inc. All rights reserved.
doi:10.1016/j.rse.2006.06.017

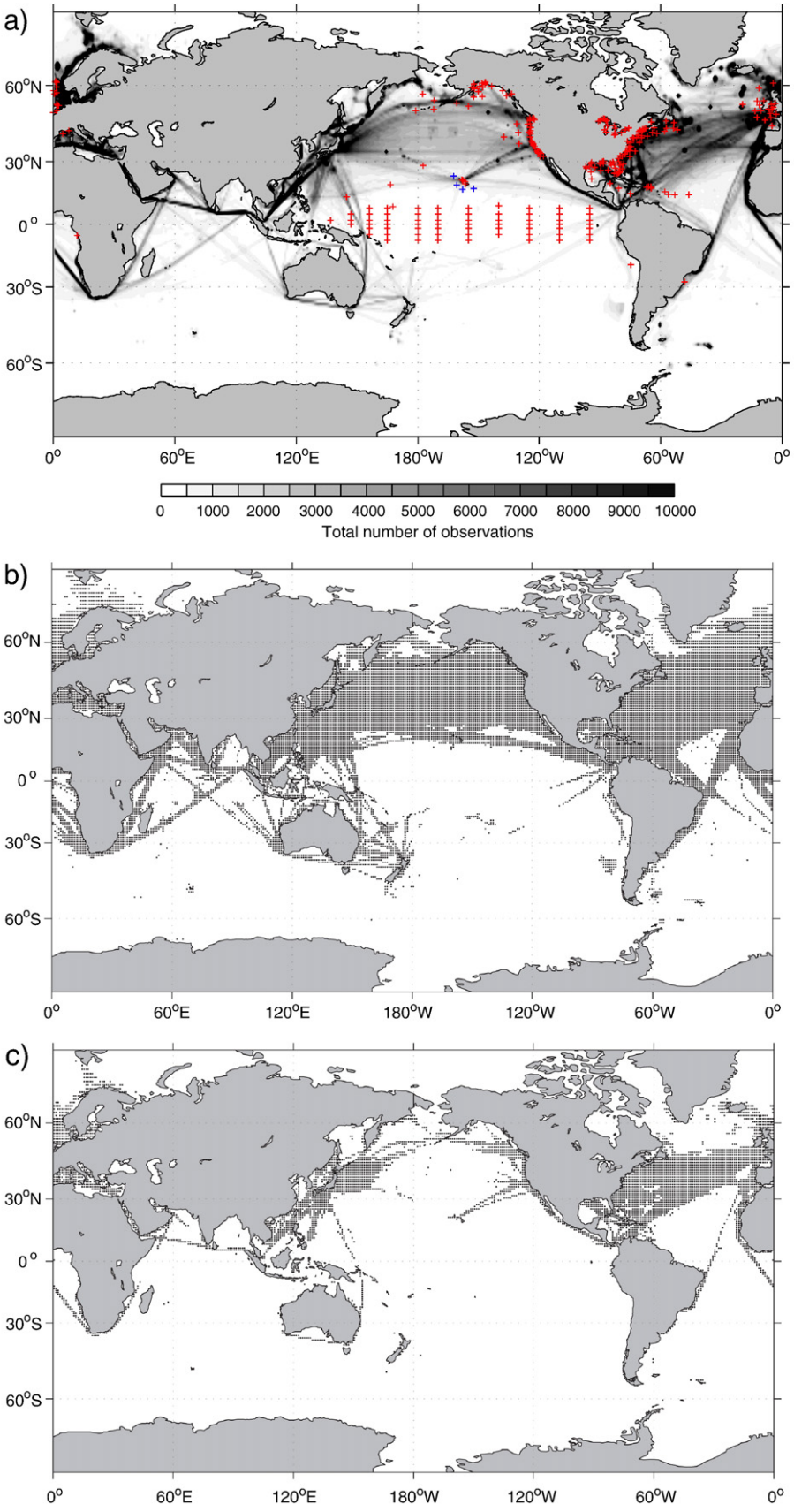
a)
60°N
30°N
0°
30°S
60°S
0°
60°E
120°E
180°W
120°W
60°W
0°
0 1000 2000 3000 4000 5000 6000 7000 8000 9000 10000
Total number of observations
b)
60°N
30°N
0°
30°S
60°S
0°
60°E
120°E
180°W
120°W
60°W
0°
c)
60°N
30°N
0°
30°S
60°S
0°
60°E
120°E
180°W
120°W
60°W
0°

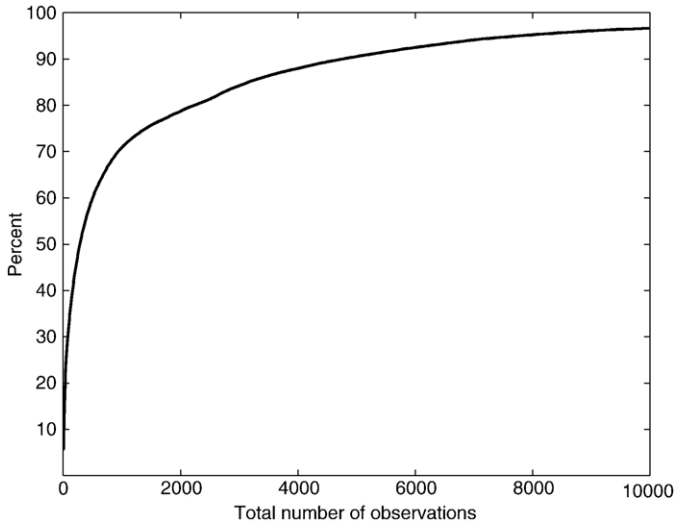

Fig. 2. The cumulative distribution function for the total number of wind observations (January 1960–December 1997) contained within each 1°×1° COADS grid cell. Note that about 70% of grid cells have a total of less than 900 observations.

1°×1° or a 5°×5° grid. Surface variables contained within this atlas include the means and standard deviations of wind speed, sea-level pressure, and air and sea-surface temperatures. These winds are derived from the Pilot Chart Global Sums Atlas and the World Marine Surface Atlas that are based on ship observations from January 1850 through December 1970.

The ASMD94 atlas presents monthly fields of zonal and meridional wind components, air and sea surface temperature, and sea-level pressure on a global 1°×1° grid. These fields are derived from the COADS Release 1 dataset (Slutz et al., 1985; Woodruff et al., 1987). The majority of observations included in COADS are obtained from the ships of the Voluntary Observing Fleet. Observations from military ships, ocean weather ships, light ships, research vessels, buoys, and bathythermographs are also included in this historical collection. Although COADS includes observations as far back as 1854, the ASMD94 climatology is based only on the years 1945 through 1989.

Both the MCA and ASMD94 atlases provide users with global climatologies of ocean winds that extend back more than 50 years. An important limitation of these climatologies is that they are derived primarily from ship measurements. Apart from the fact that ship observations are poorly sampled both spatially and temporally (Figs. 1 and 2), such measurements are contaminated by erroneous trends. These trends, which include the apparent strengthening of wind over the South China Sea, North Pacific and North Atlantic shipping lanes between 1950 and 1984, principally are thought to result from changes in measurement techniques (Cardone et al., 1990). Over this period, ship reports became increasingly based on anemometer readings, rather than sea-state estimates. Though probably more precise than subjectively estimated winds based on sea-state conditions, anemometer-based wind estimates themselves are fraught with error, including poor instrument calibration, flow distortion effects, improper averaging intervals, and incorrect subtraction of ship velocities when calculating the true wind (Cardone et al., 1990). Using 4 months (January and July 1980 and 1993) of COADS data, gridded to a 30°×30° grid, Kent et al. (1999) determined the mean random observational error for 10-m corrected ship-based wind speed measurements, between 45°S and 75°N, to be 2.1±0.2 m/s.

In contrast to the aforementioned climatologies, the 5-year QuikSCAT-based Climatology of Global Ocean Winds presented here provides, on a 0.5°×0.5° grid, densely sampled (in both space and time) wind observations that have an accuracy comparable to well-calibrated buoy observations (Chelton & Freilich, 2005; Freilich & Dunbar, 1999; Stoffelen, 1998). This spatial resolution is effectively equivalent to having approximately 150,000 buoys distributed uniformly across the global oceans.

This work was initially motivated by the National Oceanic and Atmospheric Administration's (NOAA) Office of Response and Restoration's (OR&R) need for a comprehensive atlas of global surface winds over the oceans. By providing the first global high spatial resolution, observationally based, atlas of ocean winds, COGOW will assist OR&R in fulfilling its mission of protecting and restoring NOAA trust resources as well as assisting with their international response efforts in isolated and remote regions, such as the Galapagos Islands (Sanderson et al., 2001). In addition, it is anticipated that COGOW will be useful to OR&R and the National Weather Service (NWS) for both training purposes and emergency response planning.

COGOW is introduced in Section 2 along with a brief overview of scatterometry, a detailed description of the satellite data that are included in this climatology, and a summary of data interpretation. In Section 3, a case study of NOAA OR&R's involvement in the recovery of the vessel *Ehime Maru* is presented to help familiarize users with COGOW and to illustrate one of the many potential uses of this product. Evidence of air–sea interactions over the southwest Indian and southeast Atlantic Oceans, and in the northwest Atlantic Ocean is presented in Section 4 to highlight some of many small-scale wind phenomena that are visible within COGOW. Potential user groups are discussed in Section 5 and conclusions are summarized in Section 6.

2. Data and methods

2.1. SeaWinds on QuikSCAT

The wind observations used to construct the COGOW climatology were measured by the SeaWinds scatterometer that

Fig. 1. The top panel (a) shows the total number of wind observations (January 1960–December 1997) contained within the 1°×1° Comprehensive Ocean–Atmosphere Data Set (COADS) Release 1. The increment between gray shades is 500 observations. Note the Northern Hemisphere sampling bias in both ship and buoy observations. The red crosses indicate buoys locations. The four blue crosses, in the vicinity of the Hawaiian Islands locate the positions of National Data Buoy Center (NDBC) buoys 51001, 51002, 51003, and 51004, discussed in Section 3.2. The data for all indicated buoys are available from the NDBC (http://www.ndbc.noaa.gov). The middle panel (b) shows the locations of COADS grid cells that have an average sampling rate that equals or exceeds twice per month for the 38-year period January 1960–December 1997. The bottom panel (c) shows the locations of COADS grid cells that have an average sampling rate that equals or exceeds once per 3 days for the above 38-year period.

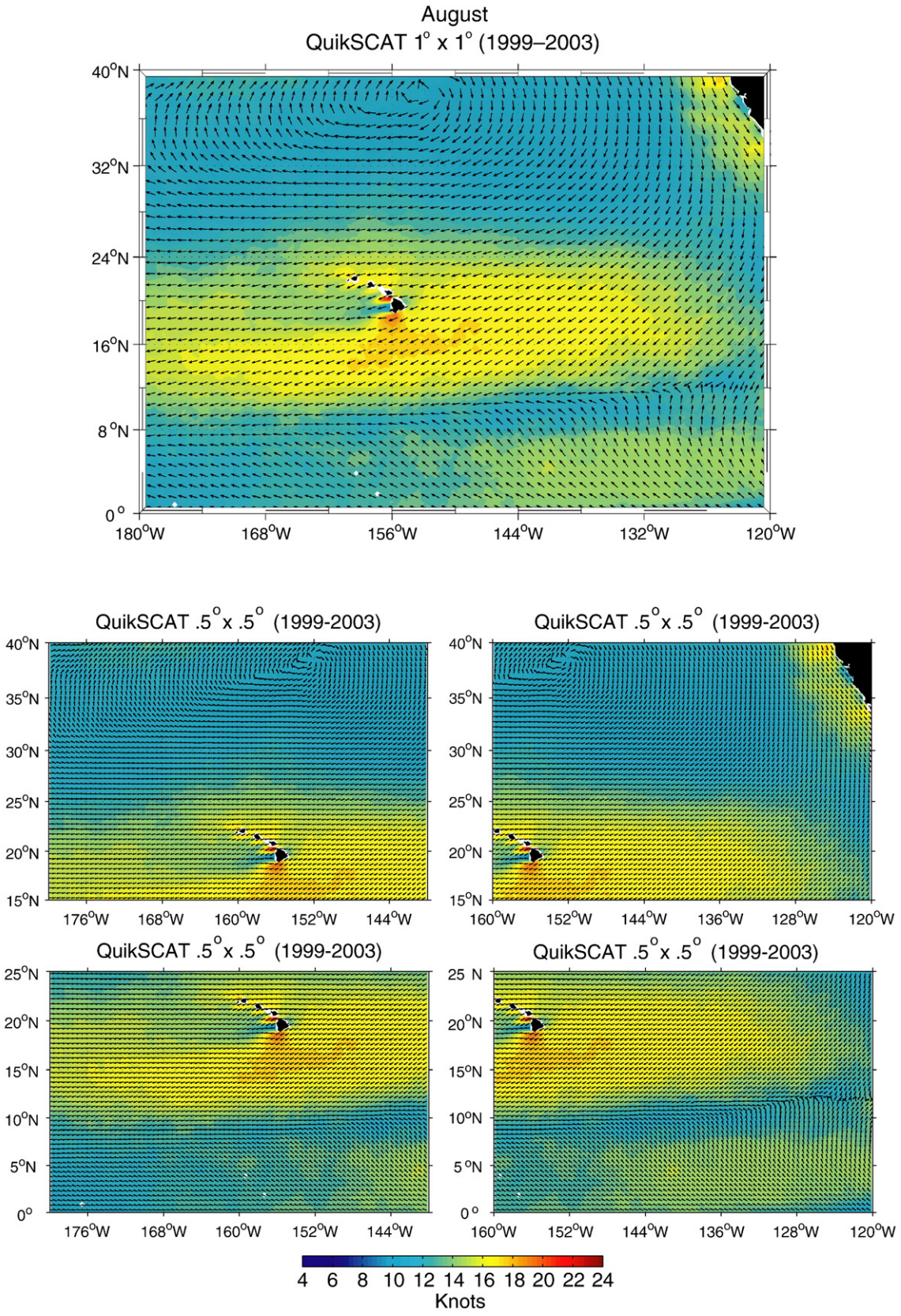

Fig. 3. The COGOW August composite average (1999–2003) of the wind field at 10 m derived from the QuikSCAT scatterometer. Scalar averaged wind speed is shown in color on a 0.25°×0.25° grid. Vector averaged climatological wind directions are plotted as unit vectors in the top panel (or regional map) on a 1°×1° grid. In the four lower panels, vector averaged climatological wind directions are plotted as unit vectors on a 0.5°×0.5° grid. Each of the four lower panels (or sub-regional maps) overlaps adjacent panels by 10° of latitude and 20° of longitude.

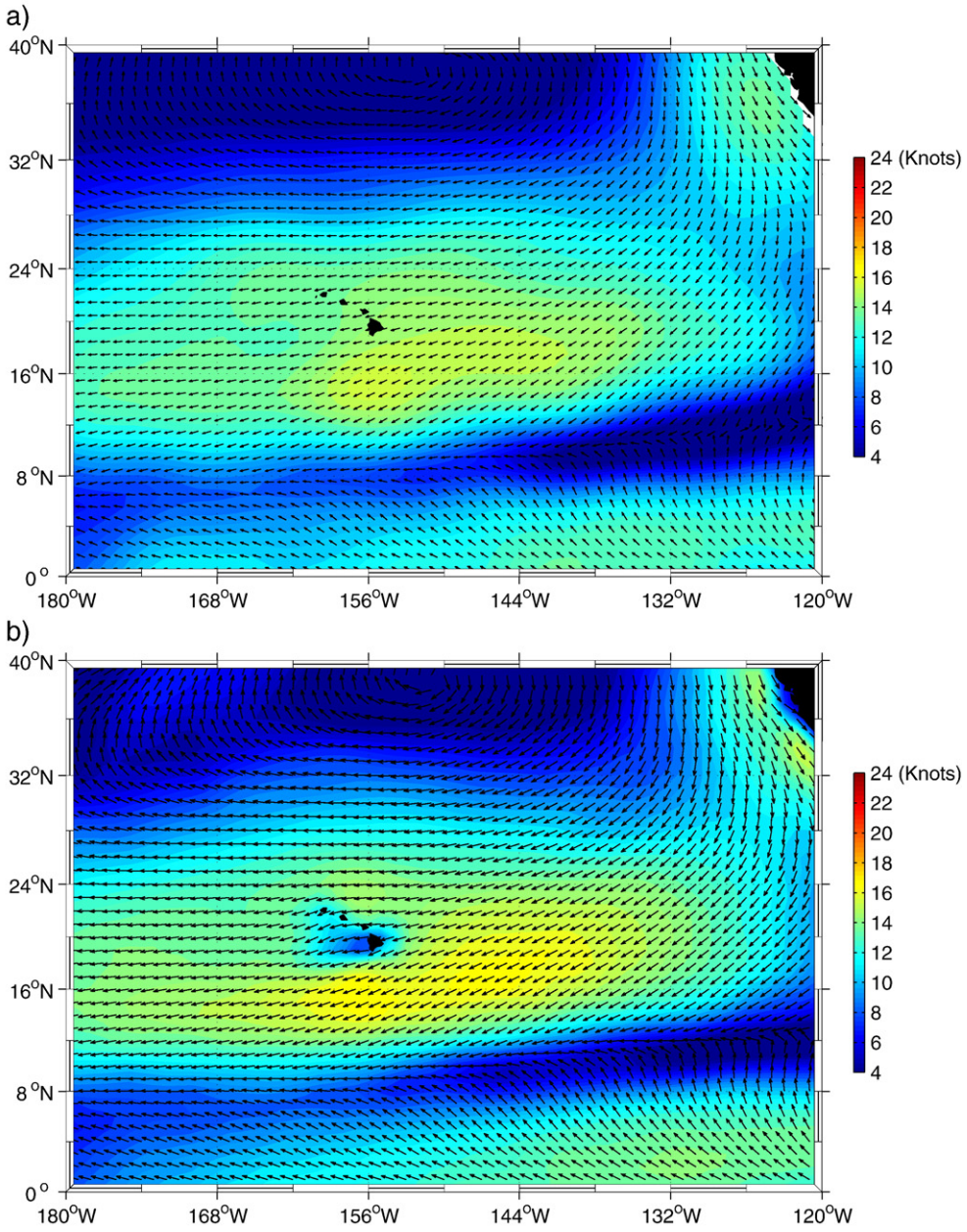

Fig. 4. The top panel (a) shows the August composite average (1945–1989) of the wind field derived from the ASMD94 climatology. Scalar averaged wind speed is shown in color on a 1°×1° grid. Vector averaged climatological wind directions are plotted as unit vectors on a 1°×1° grid. The lower panel (b) shows the August composite average (2000–2005) of the wind field derived from the NCEP operational global forecast model fields. Scalar averaged wind speed is shown in color on a 1°×1° grid. Vector averaged climatological wind directions are plotted as unit vectors on a 1°×1° grid.

was launched on 19 June 1999 onboard the QuikSCAT satellite. The geophysical data record began on 15 July 1999. The 5-year data record presented here extends from 01 August 1999 through 31 July 2004. These data were obtained from Remote Sensing Systems[1] as daily averages on a 0.25°×0.25° grid.

The QuikSCAT mission was a "quick recovery" mission to fill the gap created by the loss of the NASA Scatterometer (NSCAT) in June 1997 after only 9 months of operation. The polar orbiting QuikSCAT satellite is in a sun-synchronous orbit, 803 km above the earth's surface. With an orbit period of 101 min and an effective swath width of 1600 km, QuikSCAT is able to sample about 90% of the global oceans daily (Schlax et al., 2001). As a result of side lobe contamination, the QuikSCAT measurements analyzed for this study cannot be obtained closer than 30 km to land.

The SeaWinds scatterometer is a scanning microwave radar that measures electromagnetic backscatter from the wind-roughened ocean surface at multiple antenna look angles to infer surface wind stress magnitude and direction (Chelton & Freilich, 2005; Freilich et al., 1994). The geophysical product of the scatterometer is calibrated to the equivalent neutral-stability

[1] http://www.remss.com/.

wind at a height of 10 m above the sea surface, i.e., the wind at a height of 10 m that would produce the observed wind stress if the atmosphere were neutrally stratified. The equivalent neutral stability wind at 10 m is typically about 0.5 m/s higher than the actual wind at 10 m, and seldom differs from the actual wind at 10 m by more than 1.5 m/s (Mears et al., 2001).

The accuracy of the QuikSCAT wind retrievals is best characterized in terms of random component errors (Freilich & Dunbar, 1999). In an analysis that extends the isotropic random component error model of Freilich (1997) and Freilich and Dunbar (1999) to include anisotropy, Vanhoff and Freilich (2006, manuscript in preparation; see also the discussion in Chelton & Freilich, 2005) conclude that QuikSCAT data have random component error magnitudes of about 0.75 m/s in the along-wind direction and 1.50 m/s in the crosswind direction. Assuming the component errors are uncorrelated, the wind speed accuracy is therefore about 1.7 m/s at all wind speeds, or equivalently, about 3.3 knots. Wind direction accuracy increases significantly with increasing wind speed. For winds higher than about 6 m/s, the anisotropic component errors correspond to a directional accuracy of about 14° (Chelton & Freilich, 2005).

For more detailed discussions of scatterometry and the issues involved in the sampling of scatterometer data, the reader is referred to Chelton and Freilich (2005) and Schlax et al. (2001), respectively.

2.2. Monthly composite maps and wind rose plots

COGOW consists of two types of climatologies: 5-year monthly composite maps of scalar averaged wind speed and vector averaged wind direction, and monthly composite wind rose plots showing the 5-year climatology of relative wind speed and wind direction within 0.5° × 0.5° grid cells.

Fig. 3 shows an example of a regional COGOW 5-year monthly composite map for a 40° of latitude by 60° of longitude region centered on Hawaii for the month of August (1999–2003). The colors represent wind speed in knots plotted on a 0.25° × 0.25° grid[2]. The vector averaged climatological wind directions are plotted as unit vectors in the COGOW map (top panel) on a 1° × 1° grid. In the COGOW 25° of latitude by 40° of longitude sub-regional maps (four lower panels), vector averaged climatological wind directions are plotted as unit vectors on a 0.5° × 0.5° grid. Each sub-regional map panel overlaps adjacent sub-regional maps by 10° of latitude and 20° of longitude.

For comparison, Fig. 4a shows an example of the ASMD94 45-year monthly composite map for August (1945–1989). The colors represent wind speed in knots plotted on a 1° × 1° grid. Vector averaged climatological wind directions are plotted as unit vectors on a 1° × 1° grid. While the course resolution ASMD94 August wind field captures the approximate locations of both the Inter-Tropical Convergence Zone (ITCZ) and the North Pacific Subtropical High centered at about 40°N, 150°W, it was not able to resolve the small-scale wind structure found in the vicinity of the Hawaiian Islands. In particular, the corner acceleration south of the island of Hawaii, the inter-island gap wind accelerations, and the wind shadows present in the lee of each of the Hawaiian Islands are not resolved by the ASMD94 August wind field shown in Fig. 4a. In addition, the ASMD94 climatology underestimates wind speed regionally by up to 50%.

The wind rose plots presented in COGOW are created from temporally and spatially smoothed QuikSCAT wind fields. Daily wind fields were first constructed by vector averaging all rain-free QuikSCAT wind velocity measurements centered in each 0.25° × 0.25° bin. Rain contaminated cells were identified using the rainflag developed by Remote Sensing Systems, which is an improved version of the Empirically Normalized Objective Function rainflag described by Mears et al. (2000). The QuikSCAT sampling results in an average of 1–2 daily measurements in each bin, although incomplete global coverage and rain contamination result in some bins being sampled less frequently, while swath overlaps from consecutive orbits yield larger daily sampling poleward of about 50° latitude (Schlax et al., 2001). These daily wind fields were temporally averaged to 3-day intervals. For example, the wind field for 1 January is a composite of the wind fields for 30 December through 1 January. Similarly, the wind field for 2 January is a composite of the wind fields for 31 December through 2 January. January therefore contains 31 overlapping 3-day temporally averaged wind fields at daily intervals. While the 3-day temporal averaging removes most of the gaps in the daily wind fields, it also tends to reduce the number of directional bins in the wind rose plots in regions of high variability, and to bias the wind speed somewhat low. This is particularly true in high-latitude regions such as the Southern Ocean, and the North Pacific and North Atlantic Oceans that experience high variability on daily time scales. The QuikSCAT data were spatially averaged on to a 0.5° × 0.5° grid to reduce the data density.

Wind rose plots were constructed by sorting the temporally and spatially averaged observations into six wind speed bins with lower limits of 0, 5, 10, 15, 20 and 25 knots, and sixteen non-overlapping directional bins of width 22.5°. The “north” bin, for example, includes observations with direction from 11.25° west of north to, but not including, 11.25° east of north. The wind direction is defined by the meteorological convention as the direction from which the winds are blowing.

Wind rose plots (Fig. 5) summarize the occurrence of overlapping 3-day average winds within each 0.5° × 0.5° bin, showing their strength, direction and relative frequency. The length of each radial barb indicates the relative frequency of winds from that direction. For example, if the barb representing winds blowing from the north–northwest is twice as long as the barb representing northerly winds, the winds blew from the north-northwest twice as frequently as they did from the north.

For each directional bin in the wind rose, the barb’s appearance varies through several styles in sequence. The

[2] COGOW was originally developed to support NOAA users. The non-SI units used throughout this study reflect the fact that NOAA databases are in nautical miles and knots (nautical miles per hour). Non-SI units of measurement used here can be converted to SI units as follows:

- 1 nautical mile = 1.85 km,
- 1 knot = 1.17 mile/h = 1.88 km/h = 0.51 m/s.

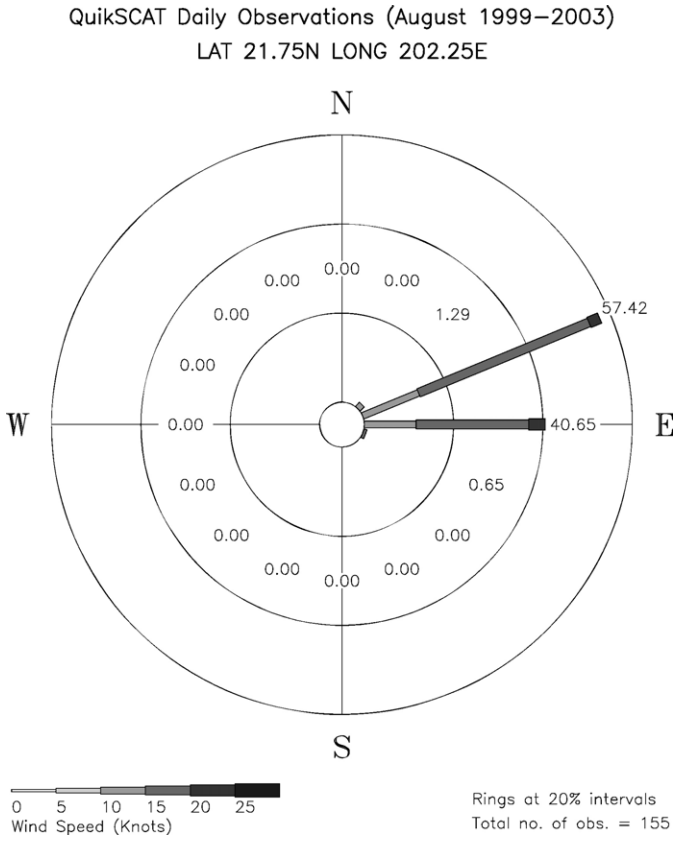

Fig. 5. The COGOW climatological wind rose plot for the month of August (1999–2003) for the 0.5°×0.5° area centered at 21.75°N and 157.75°W off the Hawaiian island of Oahu. See Table 1 for a tabular version of these data.

Table 1
Tabular form of the August data presented graphically Fig. 5

Wind direction vs. speed from QuikSCAT daily observations (August 1999–2003)							
LAT 21.75N LONG 202.25E							
Total number of observations = 155							
Wind Spd (knots)	0.0 <=	5.0 <=	10.0 <=	15.0 <=	20.0 <=	25.0 <	Total percent
Meteorological Wind Dir							
N	0.00	0.00	0.00	0.00	0.00	0.00	0.00
NNE	0.00	0.00	0.00	0.00	0.00	0.00	0.00
NE	0.00	0.00	1.29	0.00	0.00	0.00	1.29
ENE	0.00	0.00	13.55	41.29	2.58	0.00	57.42
E	0.00	0.00	11.61	25.16	3.87	0.00	40.65
ESE	0.00	0.00	0.00	0.65	0.00	0.00	0.65
SE	0.00	0.00	0.00	0.00	0.00	0.00	0.00
SSE	0.00	0.00	0.00	0.00	0.00	0.00	0.00
S	0.00	0.00	0.00	0.00	0.00	0.00	0.00
SSW	0.00	0.00	0.00	0.00	00.0	0.00	0.00
SW	0.00	0.00	0.00	0.00	0.00	0.00	0.00
WSW	0.00	0.00	0.00	0.00	0.00	0.00	0.00
W	0.00	0.00	0.00	0.00	0.00	0.00	0.00
WNW	0.00	0.00	0.00	0.00	0.00	0.00	0.00
NW	0.00	0.00	0.00	0.00	0.00	0.00	0.00
NNW	0.00	0.00	0.00	0.00	0.00	0.00	0.00
Total percent	0.00	0.00	26.45	67.10	6.45	0.00	100.00

proportion of the barb's length in each style indicates the fraction of time winds blew from that direction at a given speed. For example, a thin, light gray rectangle extending from the center indicates wind speeds between 0 and 5 knots. A slightly thicker, and slightly darker gray segment indicates wind speeds between 5 and 10 knots, and so forth until, finally, a thick black rectangle indicates wind speeds greater than 25 knots. Concentric axes at 20% frequency intervals are plotted on each wind rose. Additionally, the total number of overlapping 3-day average observations used to create each wind rose is labeled in the lower right-hand-corner of each plot.

For the month of August shown in the example wind rose in Fig. 5, the winds in the 0.5°×0.5° bin centered at 21.75°N, 157.75°W blew from the east–northeast and from the east for 57.42% and 40.65% of the time, respectively. The winds that blew from the east–northeast did so at speeds between 15 and 20 knots for about 40% of the time, almost twice as frequently as easterly winds within the same wind speed bin (Table 1). Table 2 shows an extract of the daily data used to create Fig. 5 and Table 1, illustrating the formatting that is applied to all of the "raw" wind data files for all months and locations. These files, which can be downloaded from COGOW as described in Section 3.3, are comma delimited ASCII (American Standard Code for Information Interchange) text files that contain a two-line header that gives the date and location, followed by the overlapping 3-day average winds at daily intervals tabulated as date (dd/mo/yy), wind speed and wind direction. Missing observations are reported as NaN (Not a Number). The *filename*.csv file format can be imported into spreadsheet applications such as Microsoft Excel with relative ease.

For comparison, the MCA August (1950–1970) wind rose for the 1°×1° bin centered at 21.5°N, 157.5°W is shown in Fig. 6, which is interpreted as follows: the average wind speed for all wind directions is indicated in the center of the circle. The length of each barb indicates the relative frequency of winds from that particular direction. Frequencies greater than or equal to 5% are

Table 2
An extract of the daily averaged wind speed and wind direction data used to create both Fig. 5 and Table 1

QuikSCAT Daily Observations (August 1999–2003) 21.75N_202.25E
01August99, 13.6, 254.0
02August99, 12.2, 256.5
03August99, 12.3, 260.5
04August99, 14.6, 276.0
05August99, 16.4, 271.0
06August99, 18.2, 271.5
07August99, 18.0, 254.5
08August99, 17.2, 255.0
09August99, 17.2, 254.0
10August99, 16.4, 259.5
11August99, 15.9, 255.5
12August99, 16.0, 259.0
13August99, 16.8, 258.5
14August99, 17.3, 263.0
15August99, 18.6, 259.0
…
01August00, 11.9, 228.0
…
31August03, 14.2, 266.0

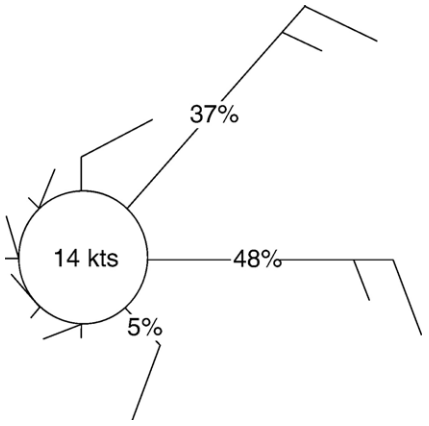

Fig. 6. Wind rose plot for the month of August (1850–1970) from the MCA climatology for the 1°×1° area centered at 21.5°N and 157.5°W.

shown as a percentage directly on the barb. The "feathers" on the end of each barb denote the average wind speed for a given wind direction. A short feather indicates an average wind speed of 5 knots, while a long feather indicates an average wind speed of 10 knots. Fig. 6 indicates that winds blew from the east and from the northeast for 48% and 37% of the time, respectively. The average wind speed for both east and northeast winds was 15 knots and the average wind speed for all wind directions was 14 knots.

Compared with the COGOW wind rose in Fig. 5, the MCA wind rose in Fig. 6 contains three notable weaknesses. Firstly, it contains only eight directional bins, whereas COGOW contains 16 directional bins. As a consequence, the MCA climatology suggests that 37% of the August winds blow from the northeast, whereas COGOW indicates that the winds at this location almost never blow from the northeast. Secondly, it contains no information on the distribution of wind speeds, showing only the average wind speed for each of the eight directional bins. Lastly, the MCA wind rose does not show the number of observations that were included in the plot.

While ASMD94 provides monthly gridded fields of zonal and meridional wind components, it is noteworthy that it does not include monthly composite wind rose plots. In contrast, MCA provides monthly composite wind rose plots but does not include monthly gridded wind fields of any kind. The COGOW climatology presents both gridded monthly composite fields of wind speed and direction and monthly composite wind rose plots on a 0.5°×0.5° global grid.

3. Climatology of Global Ocean Winds (COGOW)

3.1. About COGOW

The web-based COGOW interactive atlas, which is accessible at URL http://cioss.coas.oregonstate.edu/cogow, allows users to retrieve scatterometer-derived climatological average wind statistics for each calendar month, in both tabular and graphical form, for most ocean regions of interest on a 0.5°×0.5° grid. While this climatology is accessible via all modern web browsers, it is best viewed at a screen resolution of 1600×1200 DPI (dots per inch) using the Firefox or latest Netscape web browsers.[3] Minor technical problems occur with Microsoft Internet Explorer, as summarized below in Section 3.3. The screen resolution of 1600×1200 DPI was adopted as a compromise between website design/layout and monthly composite map visualization. This climatology is not optimized for lower-resolution computer monitors such as laptop computers.

3.2. The Ehime Maru

As an example application of COGOW, we consider NOAA OR&R's involvement in the recovery of the Japanese training and fishing vessel *Ehime Maru*. On 09 February, 2001, *USS Greeneville*, a Los Angeles class submarine, collided with *Ehime Maru* approximately 17 km south of Diamond Head on the island of Oahu, Hawaii. *Ehime Maru* sank in about 600 m of water. At the time of sinking, 26 of the 35 crewmembers were rescued. The U.S. Navy was unable to locate the nine remaining crewmembers. It was presumed that they were trapped inside the vessel or went overboard as the ship sank. Following communications with the Japanese government, the U.S. Navy agreed to attempt to recover *Ehime Maru* and the nine missing crewmembers, their personal effects, and certain unique ship components (Department of Defense, 2001).

Prior to the recovery effort, the mandates of the National Environmental Policy Act (NEPA) of 1969 required the U.S. Navy to prepare an environmental assessment (EA). The EA evaluated the potential environmental impact of the U.S. Navy's proposal to lift *Ehime Maru* from the seafloor, transport the vessel to a shallow-water site in order to recover the crewmember remains, and then permanently relocate the ship to a deep-water site. This EA resulted in a finding of no significant impact (Department of Defense, 2001).

Based on the EA, Reef Runway, located to the southeast of Pearl Harbor, was selected as the preferred shallow-water recovery site (Fig. 7). NOAA OR&R ran a series of oil plume trajectory analyses to model the behavior of a potential uncontained diesel fuel release at Reef Runway. Several variables, including wind direction and tidal flow, were incorporated into each model analysis. Model constants included wind speed (assumed to be 10 knots) and the amount of diesel fuel released (76,000 l) (Department of Defense, 2001). NOAA OR&R's use of a 10-knot wind speed was based on the 10-year average August wind speed recorded at the Honolulu International Airport weather station located at 21.35°N, 157.93°W, approximately 30 km north-northwest of the location where *Ehime Maru* initially sank. The instantaneous fuel release of 76,000 l was considered to be the most realistic amount of diesel fuel that could leak in the event of a ruptured fuel tank. The models were run for a 24-h period (Department of Defense, 2001).

Results from NOAA OR&R's Reef Runway model analyses concluded that easterly winds could result in diesel fuel being pushed toward the beach at Barbers Point during both ebb and flood tide conditions (top panels of Fig. 7). East–northeast winds could also result in diesel fuel being pushed toward the

[3] Firefox is available free from http://www.mozilla.com/firefox/. Netscape is available free from http://browser.netscape.com/.

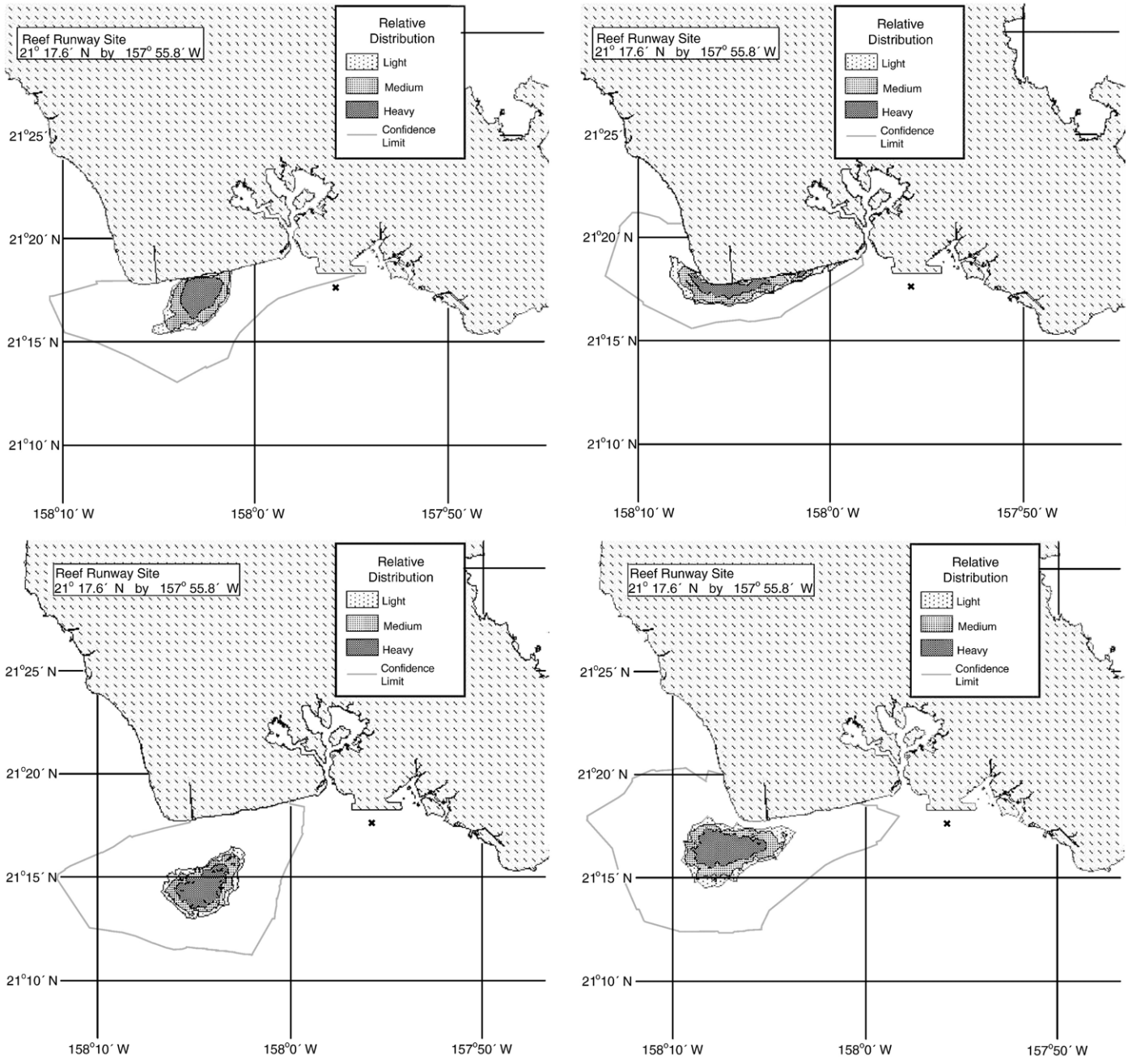

Fig. 7. The NOAA OR & R trajectory analyses for the Reef Runway shallow-water recovery site indicated by a cross to the southeast of Pearl Harbor. The top panels show the results of the ebb (left) and flood (right) tide analyses that were forced with a 10 knot easterly wind. The bottom panels show the results of the ebb (left) and flood (right) tide analyses that were forced with a 10 knot east-northeasterly wind. (Modified from Department of Defense, 2001.)

beach during both tidal extremes, although more likely during flood conditions (bottom panels). North–northeast winds were expected to force the plume offshore under all tidal conditions (not shown).

NOAA OR&R's use of a constant wind speed based on the 10-year average August wind speed recorded at the Honolulu International Airport raises the following questions:

1. How representative is the assumed wind speed of 10 knots?
2. How variable is the ocean surface wind field off the island of Oahu in terms of wind direction for the month of August?

To answer these questions, NOAA OR&R might have considered data derived from the four National Data Buoy Center (NDBC) buoys 51001 (23.43°N, 162.21°W), 51002 (17.14°N, 157.79°W), 51003 (19.16°N, 160.74°W), and 51004 (17.52°N, 152.48°W), located offshore of the Hawaiian Island chain and shown by the blue crosses in Fig. 1a; however, all of these buoys are situated a considerable distance offshore of Oahu, and it can therefore be argued that consideration of the buoy data would be ineffectual with respect to the nearshore recovery effort of *Ehime Maru*. They might also have analyzed the wind fields from the National Centers for Environmental

Predication (NCEP) operational global forecast model, but as shown in Fig. 4b, these model fields are not able to resolve features with scales smaller than about 500 km (Chelton et al., 2006; Milliff et al., 2004), despite a model grid resolution of about 50 km. The NCEP model therefore smears the small-scale local wind features that may be critical to oil plume trajectory modeling.

The following section details how access to the COGOW climatological wind atlas would have been useful in NOAA OR&R's modeling of a potential oil spill during the *Ehime Maru* recovery operation and serves as a brief tutorial on the use of COGOW.

3.3. Becoming familiar with COGOW

The COGOW interactive atlas is launched by typing the URL http://cioss.coas.oregonstate.edu/cogow/ into the address field of a web browser. The homepage of COGOW consists of the map shown in Fig. 8.[4] The map in Fig. 8 is divided into seventy-seven 40° latitude by 60° longitude regional maps, which become apparent as blue bounding boxes when the cursor is moved over the image. Each regional map overlaps adjacent regional maps by 20° of latitude and 30° of longitude. Left-clicking on one of these regions displays the January climatological average wind map of scalar averaged wind speed and vector averaged wind direction on a $1° \times 1°$ grid. As shown by the example in Fig. 3, each of these regional maps is further subdivided into four overlapping sub-regional maps spanning 25° of latitude and 40° of longitude that depict climatological average winds on a finer $0.5° \times 0.5°$ grid.

Left-clicking on the region shown in Fig. 8 displays the January (2000–2004) average map analogous to the August map shown in the top panel of Fig. 3 for the region near Hawaii that is of interest for the *Ehime Maru* study. The climatological mean month-to-month variability observed in the 5-year QuikSCAT data for this region can be seen by left-clicking, in sequence, on each of the month tabs (January–December) located directly above the initial January regional map. The northward retreat of the westerly wind belt with the onset of the boreal spring and summer is evident from this sequence of twelve maps. Commensurate with this retreat is the seasonal variation of the latitude of the ITCZ, located between the equator and 9°N. Summer winds (May through August) are seen to be about 50% weaker than those of the winter months. An exception to this can be seen in the top right corner over the California Current, as well as in the Alalakeiki Strait that separates the islands of Hawaii and Maui. The large-scale anticyclonic circulation that is associated with the North Pacific Subtropical High centered at about 40°N, 150°W is also apparent in the COGOW regional maps for the months of July and August.

The QuikSCAT climatological average August wind field (top panel of Fig. 3) for the region around Hawaii can viewed by left-clicking on the "August" tab. As noted previously, this regional map is subdivided into four overlapping sub-regional maps. Left-clicking on a point south of the island of Oahu zooms in on the location where *Ehime Maru* sank displays the high-resolution sub-regional climatological mean map for the month of August shown in the top left sub-regional panel of Fig. 3.[5] Running the cursor over this sub-regional map produces a wind rose plot to the right of the map like that shown in Fig. 5. The wind rose display changes in real time as the position of the cursor changes. Placing the cursor on the wind vector situated directly south of the island of Oahu (21.75°N, 157.75°W) produces the wind rose plot shown in Fig. 5.

For this location, the August winds tend to blow from the east and east–northeast 40.7% and 57.4% of the time, respectively. Table 1 shows that east-northeasterly winds blow between 10 and 15 knots 13.6% of the time, between 15 and 20 knots 41.3% of the time and in excess of 20 knots 2.6% of the time. Easterly winds blow between 10 and 15 knots 11.6% of the time, between 15 and 20 knots 25.2% of the time and in excess of 20 knots 3.9% of the time.

Without moving the cursor, left-clicking on the wind vector situated directly south of the island of Oahu produces a popup box[6] that allows the user to save the wind rose in graphical (e.g., Fig. 5), tabular (e.g., Table 1) or "raw" data form (e.g., Table 2).

The COGOW climatological average August wind statistics can be used to answer the two questions posed in Section 3.2 for the NOAA OR&R analysis of possible oil spill trajectories in the recovery of *Ehime Maru*. The COGOW wind rose statistics indicate that NOAA OR&R's usage of a 10-knot wind in their modeling effort significantly underestimated typical wind speeds in this region. August wind speeds at this location are more typically between 15 and 20 knots. If anything, the COGOW value of between 15 and 20 knots may be biased somewhat low as it is derived from QuikSCAT data that are temporally averaged to 3-day composites.

With regard to wind direction, Fig. 5 shows there is low variability of wind direction at this location during August. The winds blow from either the east–northeast or east more than

[4] Macromedia Flash Player, available free from http://www.macromedia.com/go/getflashplayer/, is required to run COGOW.

[5] Clicking on a regional map using the Microsoft Internet Explorer browser will launch a popup box that states, "A script on this page is causing IE to run slowly. If it continues to run, your computer may become unresponsive. Do you want to abort the script?" Select "no" to ignore this message and continue on. The reason for this popup is that a substantial amount of JavaScript is used to render each sub-regional map. This rendering, which occurs every time one of the sub-regional maps is selected, takes about 10 s to complete. If the user wishes to remove this Microsoft limitation, the default timeout value for Internet Explorer can be changed with a straightforward modification of the system registry. A detailed discussion of this procedure is give in this Microsoft knowledgebase article http://support.microsoft.com/?kbid=175500. This limitation is not found in the Mozilla-branded browsers (Mozilla and Firefox) or later versions of the Netscape browser.

[6] This will not work with Microsoft Internet Explorer if the popup blocker is activated. This can be overcome by holding down the "Ctrl" key while left-clicking. Alternatively, the user can left-click on the "Tools" dropdown menu located at the top of the Internet Explorer window and then left-click on "Internet Options…" A popup box with a number of tabs will appear on the screen. These tabs include a "General" tab, a "Security" tab and a "Privacy" tab. Left-click on the "Privacy" tab. If the box labeled "Block pop-ups" is checked, uncheck it by left-clicking on the box and then left-click the "OK" button.

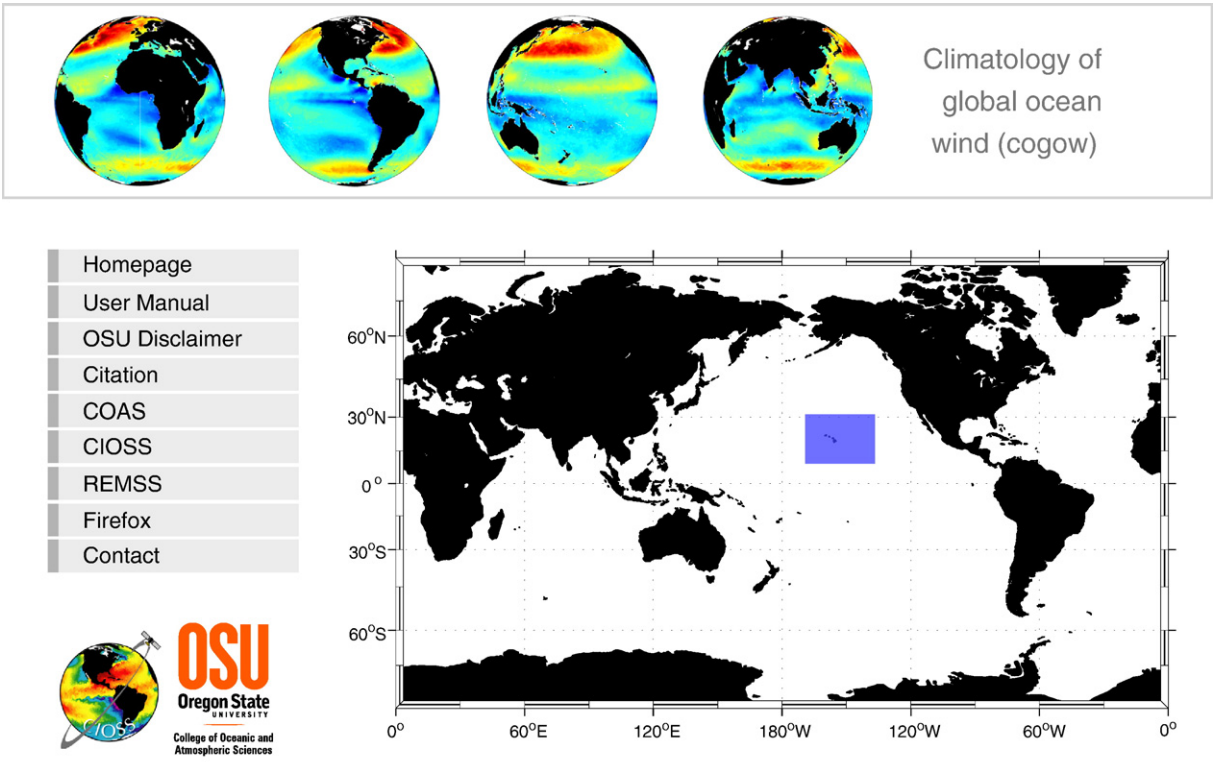

Fig. 8. A screenshot of the homepage of the Climatology of Global Ocean Winds (http://cioss.coas.oregonstate.edu/cogow). The global map is subdivided into seventy-seven, overlapping (40° latitude by 60° of longitude) regional maps. Left-clicking on any one of these regional maps displays the 5-year January climatology of ocean winds for that region derived from QuikSCAT measurements.

98% of the time. Recall that NOAA OR&R's model results (Fig. 7) showed that easterly winds would result in diesel fuel being pushed toward the beach at Barbers Point during both ebb and flood tide conditions. Likewise, east–northeast winds could potentially result in diesel fuel being pushed toward the beach during both ebb and flood tidal conditions, especially during flood conditions. From the predominance of easterly or east–northeasterly winds in the COGOW climatology for August, it thus appears from NOAA OR&R's model results that an oil spill on the beach at Barbers Point would have been highly likely if the fuel tanks of *Ehime Maru* had ruptured during the recovery operation.

4. Evidence of SST influence on the surface wind field

Many small-scale features exist in the COGOW climatological average wind fields that are not evident in previously published climatologies. For example, the narrow wind jets between the Hawaiian Islands that are clearly seen in Fig. 3 but are not evident in either the ASMD94 climatology in Fig. 4a or the NCEP climatology in Fig. 4b. Similar features are evident in many other island chains around the world oceans, especially in the tropics where the wind direction is relatively steady. In open ocean regions that contain strong sea-surface temperature (SST) fronts, small-scale spatial variability in the surface wind field is due primarily to the influence of SST (see reviews by Chelton et al., 2004; Xie, 2004). This SST influence on the surface wind field is poorly represented in global numerical weather prediction models (Chelton et al., 2006, 2004; Chelton & Wentz, 2005), resulting in overly smooth structure in the global wind field in these models. Examples of this SST influence on the surface wind field are provided below in Sections 4.1 and 4.2. If possible, this section should be read in conjunction with COGOW's online content.

4.1. Southwest Indian and Southeast Atlantic Oceans

The Agulhas Current system of the southwest Indian Ocean is a region with strong SST gradients. Annually averaged SST gradients across the Agulhas Return Current (ARC) can exceed 4 °C $(100\ \text{km})^{-1}$ (O'Neill et al., 2005). As reviewed by O'Neill et al. (2003, 2005), Xie (2004) and Chelton et al. (2004), strong ocean–atmosphere interactions are evident from satellite observations in such regions of strong SST gradients, as well as from analytical and mesoscale atmospheric models as suggested by Sweet et al. (1981), Jury and Walker (1988) and Small et al. (2005), and from climatological average ship observations (Wallace et al., 1989). SST gradients influence the marine atmospheric boundary layer (MABL) by modifying its stability through changes in air–sea heat flux. Colder waters act to stabilize the MABL. This inhibits the vertical turbulent mixing of momentum from aloft to the surface and results in a shallowing of the MABL and a deceleration of surface winds. The reverse is true of warmer waters where increased surface heat fluxes destabilize and deepen the MABL. This

destabilization enhances the vertical turbulent mixing of momentum from aloft to the surface and results in an acceleration of surface winds. Lindzen and Nigam (1987), Small et al. (2005) and Samelson et al. (2006) argue that SST-induced pressure gradients and boundary layer thickness also play important roles in the wind response to SST.

The influence of SST on surface winds is readily apparent in COGOW's 5-year mean monthly composite maps of the surface wind field. The June (2000–2004) wind speed and wind direction composite average off southern Africa is shown in Fig. 9a. Regions of lower wind speeds are visible along the south and west coasts of southern Africa. A notable isolated area of low wind speeds occurs at about 38°S, 26°E, which coincides with the position of the Agulhas Plateau, a major bathymetric obstacle that lies across the path of the ARC. A band of relatively high wind speed extends southwestward from the coast of South Africa at about 27°E. This band of relatively high wind speed is separated from the coast by an inshore region of low wind speed. The band of low wind speed

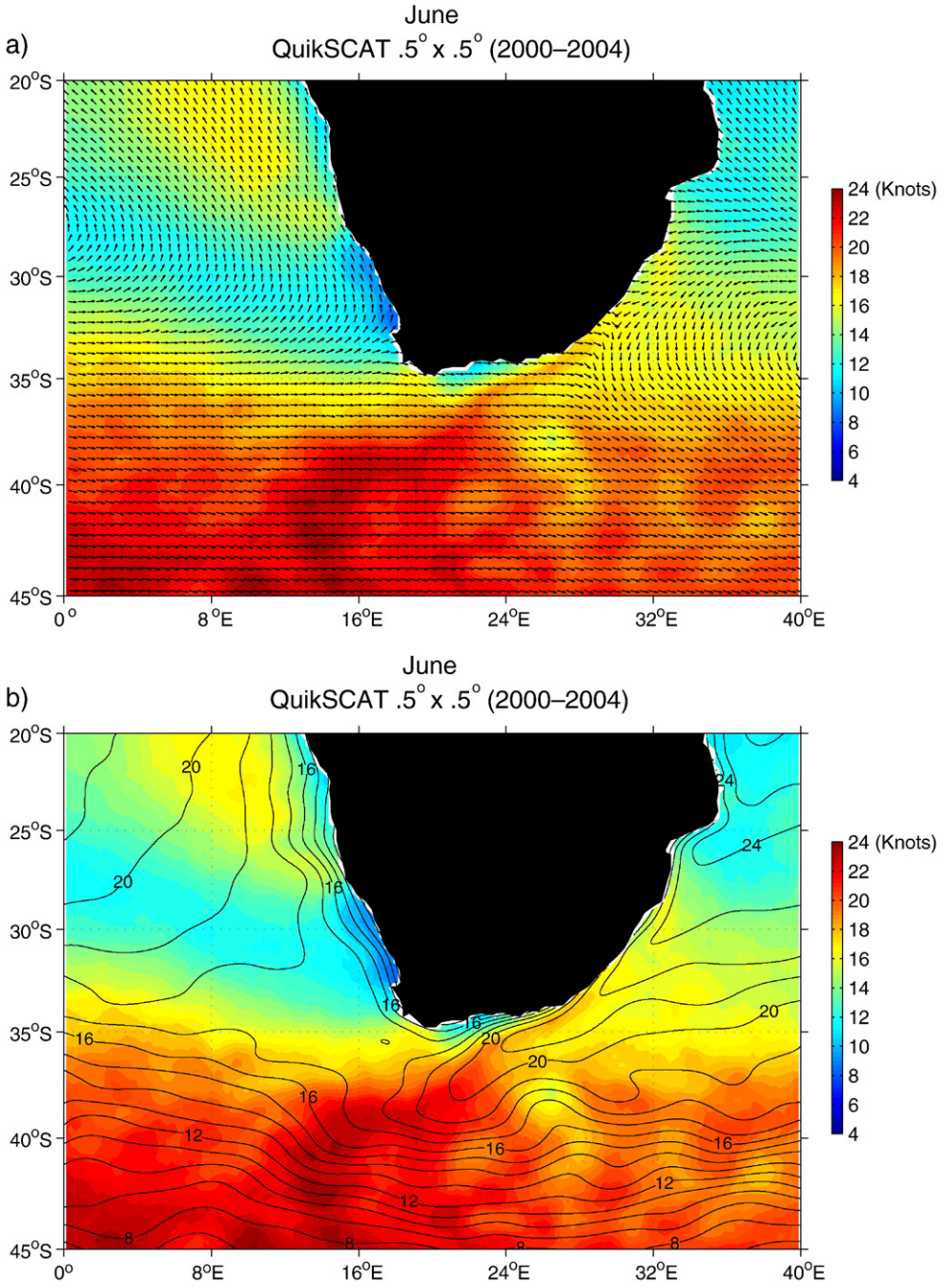

Fig. 9. The top panel (a) shows the COGOW June (2000–2004) composite average of the QuikSCAT wind field. Scalar averaged wind speed is shown in color on a 0.25° × 0.25° grid. Vector averaged climatological wind directions are plotted as unit vectors on a 0.5° × 0.5° grid. The lower panel (b) shows the COGOW June (2000–2004) composite of scalar averaged QuikSCAT 10 m wind speed in color for the southwest Indian and southeast Atlantic Oceans. Overlaid are spatially smoothed MODIS SST contours for the same five-year period with a contour interval of 1 °C.

that occurs along the west coast of southern Africa is interrupted at about 27°S by a region of relatively high wind speeds.

These small-scale structures in the surface wind field are attributable mostly to the influence of SST. The June (2000–2004) average wind speed off southern Africa is shown in Fig. 9b with contours of spatially smoothed MODIS (Moderate Resolution Imaging Spectroradiometer) SST overlaid for the same 5-year averaging period. In general, colder SSTs, such as those that occur along the west coast of southern Africa, are collocated with regions of reduced wind speeds. The northward intrusion of relatively cold SSTs at about 38°S, 26°E coincides with the previously noted patch of lower wind speeds over the Agulhas Plateau. In contrast, relatively warm SSTs, such as those associated with the Agulhas Current that flows along the southeast coast of South Africa and separates from the coast at 27°E, are collocated with regions of relatively high wind speeds.

4.2. Northwest Atlantic Ocean

The northwest Atlantic Ocean contains strong SST gradients associated with the Gulf Stream. The magnitude of these SST gradients is the same as the region considered in Section 4.1. The influence of SST perturbations on the low-level wind field is therefore also intense in the Gulf Stream region. This is clearly illustrated in Fig. 10, which shows the COGOW 5-year April (2000–2004) mean monthly composite map of surface wind speeds over the northwest Atlantic Ocean with spatially smoothed contours of MODIS SST overlaid for the same 5-year period. Regions of lower wind speed north of 42°N and in the northeast corner of the Gulf of Mexico are collocated with regions of cooler SST. Likewise, the relatively warm SST associated with the Gulf Stream is coupled with regions of higher wind speeds.

Offshore of Cape Hatteras (35.5°N, 75.5°W), Fig. 10 shows strong gradients for both SST and wind speed. SST increases offshore by about 4 °C over a distance of approximately 100 km in the April climatological average. Average wind speed increases by about 2.5 m/s over the same region. This SST-induced spatial variability can be much stronger at any particular time. The offshore increase in the 5-year April (2000–2004) climatological average wind speed across the Gulf Stream is sometimes masked by spatial variability of wind speeds associated with synoptic weather systems. For example, using data derived from a QuikSCAT overpass on 16 February 2005, Chelton et al. (2006) show wind speeds of 10–14 m/s on the south side of the North Wall of the Gulf Stream, defined to be the 17.5 °C SST isotherm, and 4–7 m/s wind speeds on the north side of the North Wall. This transition of more than 7 m/s from high to low wind speeds occurred over a distance of less than 50 km. Such short-scale wind speed variability can have a significant impact on mariners, especially those operating small fishing and sailing vessels, and search and rescue operations.

5. Potential user groups

It is clear from the *Ehime Maru* example in Sections 3.2 and 3.3 that COGOW will be very useful to oil spill responders both within the US and internationally in isolated and remote regions such as the Galapagos Islands (Sanderson et al., 2001). In addition, COGOW could be used for oil spill contingency planning purposes. For example, the Australian National Marine Oil Spill Contingency Plan (NMOSCP) states that,

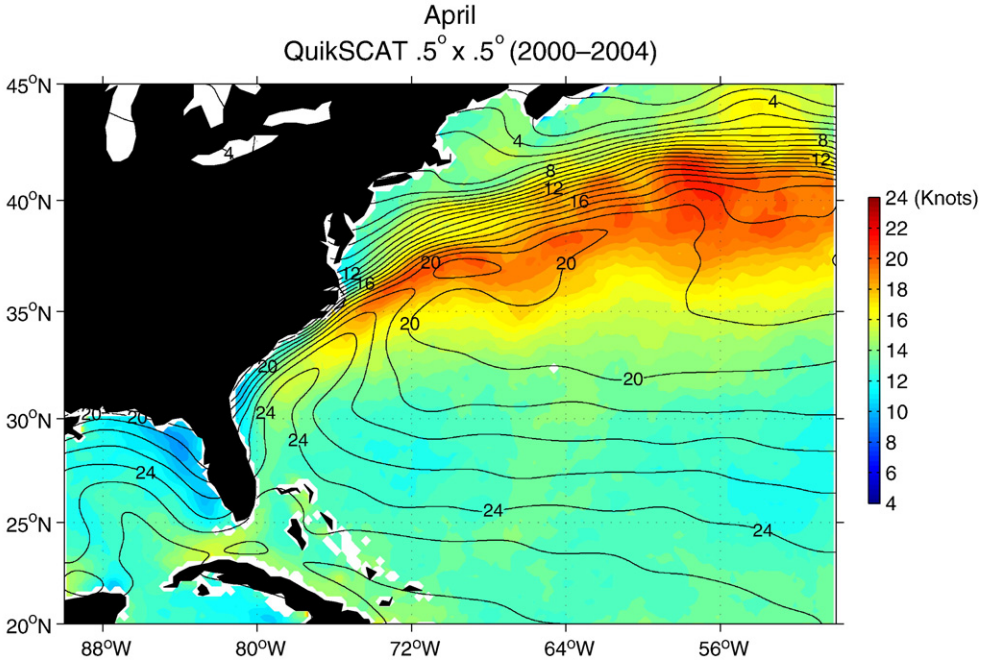

Fig. 10. The COGOW April (2000–2004) composite of scalar averaged QuikSCAT 10 m wind speed in color for the northwest Atlantic Ocean. Overlaid are spatially smoothed MODIS SST contours for the same 5-year period with a contour interval of 1 °C.

"Wind speed and direction at spill location is vital to the effectiveness of the spill simulation model" (NMOSCP, 2005). Another example of the need for high quality wind speed and direction data is given by the International Petroleum Industry Environmental Conservation Association (IPIECA), a voluntary non-profit organization whose membership includes both petroleum companies and associations at regional, national and international levels. The IPIECA suggests in their Guide to Contingency Planning for Oil Spills on Water (IPIECA, 2000) that an oil spill contingency plan should be comprised of, amongst other things, a data directory that contains relevant coastal charts including ocean current and tidal information and prevailing wind speed and direction data. COGOW fulfills the need for wind data.

COGOW is also of potential use to the private sector and to resource managers planning development of offshore wind power technologies. Musial and Butterfield (2004) estimate the wind energy potential to be in excess of 3 giga watts (GW)[7] in the area between 20 and 50 nautical miles (about 35–90 km) offshore of California and the Pacific Northwest, a region that is resolved in the QuikSCAT dataset from which COGOW was constructed.

Search and rescue (SAR) responders may also make good use of COGOW. Roper (2004) identifies the key parameters in predicting the trajectory of a SAR object as being mean surface wind and current velocities and their variability, the above- and below-water profile of the drifting object, and the last known position of the object. For most SAR operations, such data should be available within 4 h of the incident (Roper, 2004). The spatial resolution required depends upon the nature of the SAR object. For example, survival craft require lower resolution data than persons floating in the water. Presently, however, the Canadian Meteorological Center is only able to supply the Canadian Coast Guard with model wind fields on a $2° \times 2°$ grid south of 60°N and on a 2° latitude by 4° longitude grid over the Arctic (Roper, 2004). While COGOW presently provides only climatological average wind data, which are not suitable for real-time SAR operations, it is able to provide these data at a considerably higher spatial resolution ($0.5° \times 0.5°$ grid) than that of the Canadian Meteorological Center. COGOW could therefore be of use to SAR teams in support of SAR training exercises and contingency planning.

A future version of the COGOW wind maps and wind rose plots could include the option to overlay near real-time (NRT) wind vector measurements derived from QuikSCAT wind observations. In addition to satisfying the needs of SAR operations and oil spill responders, such an addition would be of significant value to commercial maritime industries and other user groups. With NRT capabilities, COGOW could be incorporated into, for example, NOAA's Physical Oceanographic Real Time System (PORTS), which is a decision support tool that is designed to improve navigation safety and efficiency. PORTS is just one of the marine navigation services offered by NOAA's National Ocean Service.

In the present configuration of COGOW, users are able to download the "raw" wind speed and direction data that were used in the creation of each of the wind rose plots, thus providing the data to calculate, for example, the 5-year seasonal cycle for a particular $0.5° \times 0.5°$ region. As the span of the data record continues to grow, researchers and managers will also be able to compare and contrast wind conditions during El Niño years and La Niña years (Rasmusson & Carpenter, 1982) or during warm and cool phases of the Pacific Decadal Oscillation (Mantua & Hare, 2002). These kinds of analyses would provide insight into wind conditions associated with the onset of these and similar climatic phenomena.

6. Conclusions

While it is clear that knowledge and understanding of global ocean winds is important at many levels within society, this comprehension has historically been hindered by poor *in situ* coverage by buoys and ships alike over most of the global oceans (Figs. 1 and 2). The Climatology of Global Ocean Winds (COGOW) presented here attempts to fill this information gap. COGOW is a 5-year (August 1999–July 2004) climatology derived from NASA's Quick Scatterometer (QuikSCAT) satellite. While other published climatologies of global ocean winds exist, COGOW provides, within the limitations of the 5-year duration of the dataset analyzed here[8], the first high spatial resolution, observationally based, online interactive atlas of global ocean winds.

Through its climatological maps and wind rose plots, COGOW provides insight into many fascinating ocean wind phenomena. One such phenomenon, the influence of SST gradients on small-scale variability of surface winds, is clearly observed in regions such as the southwest Indian and northwest Atlantic Oceans that are subject to strong SST gradients. Higher wind speeds are found to be associated with relatively warm SST. The reverse is found to be true of nearby regions that are subject to relatively cool SST. Such information could be important for search and rescue teams such as the U.S. and Canadian Coast Guards for assistance with training exercises and contingency planning.

An example of COGOW's utility to user groups such as oil spill responders and oil spill contingency planners was introduced through the case study of NOAA OR&R's involvement in the recovery efforts of *Ehime Maru*, a Japanese training and fishing vessel that sank south of the island of Oahu after it collided with the *USS Greeneville*. This case study showed that the 10-knot constant wind speed used by OR&R in their oil spill trajectory analyses, when compared with the COGOW climatology for August, significantly underestimated the average wind speeds south of Oahu. Moreover, COGOW showed the winds to contain high directional steadiness, blowing predominantly from the east or east-northeast at speeds of between 15 and 20 knots. Such information could have proven vital for oil spill mitigation, had

[7] The total U.S. electrical generation capacity for all fossil, nuclear and renewable generation is 914 GW (http://www.eere.energy.gov/windandhydro/windpoweringamerica/pdfs/workshops/2005_summit/musial.pdf).

[8] As of the time that the revision of this manuscript was finalized, QuikSCAT celebrated its seventh year in orbit.

the fuel tanks of *Ehime Maru* ruptured during the recovery operation. Examples of other potential COGOW user groups such as the private sector investors and resource managers involved in the planning and development of offshore wind power technologies were discussed.

Efforts are underway to address the limitations of COGOW. One extension under consideration is to overlay near real-time QuikSCAT wind vectors on the COGOW climatological average wind rose plots generated from daily wind speed and direction data. Another extension under consideration is implementing monthly updates of the COGOW climatological statistics. To insure its full utility, it would be useful for an interested operational agency such as NOAA to conduct needs-assessment workshops with potential research and operational users.

Acknowledgements

This research was conducted with support from NASA grant NAS5-32965 for funding of Ocean Vector Winds Science Team activities and award NA03NES4400001 to Oregon State University's Cooperative Institute for Oceanographic Satellite Studies from the National Oceanic and Atmospheric Administration, U.S. Department of Commerce. The statements, findings, conclusions, and recommendations expressed here are those of the authors and do not necessarily reflect the views of the National Oceanic and Atmospheric Administration, the U.S. Department of Commerce or the National Aeronautics and Space Administration. The QuikSCAT data presented here were produced by Remote Sensing Systems and sponsored by the NASA Ocean Vector Winds Science Team (http://www.remss.com). The gridded 4 km MODIS data were obtained from the Physical Oceanography Distributed Active Archive Center (PO.DAAC) at the Jet Propulsion Laboratory (http://podaac.jpl.nasa.gov). The authors thank Barry Vanhoff for his help in processing the gridded 1°×1° NCEP operational global forecast model fields. These fields were provided by the National Centers for Environmental Prediction (ftp://ftpprd.ncep.noaa.gov/pub/data/nccf/com/gfs/prod/). The gridded 1°×1° ASMD94 data were obtained from the IRI/LDEO Climate Data Library (http://ingrid.ldgo.columbia.edu/SOURCES/.DASILVA/.SMD94/.climatology). MCA climatology data were obtained from the National Climatic Data Center (http://ols.nndc.noaa.gov/plolstore/plsql/olstore.prodspecific?prodnum=C00454-CDR-A0001). Eric Beals is thanked for providing the wind rose plotting Fortran code. Ralph Milliff and two anonymous reviewers provided helpful comments that improved the manuscript. Lastly the authors would like to thank James Good and Michael Freilich for valuable comments on the manuscript.

References

Cardone, V. J., Greenwood, J. G., & Cane, M. A. (1990). On trends in historical marine wind data. *Journal of Climate*, *3*, 113–127.

Chelton, D. B., & Freilich, M. H. (2005). Scatterometer-based assessment of 10-m wind analyses from the operational ECMWF and NCEP numerical weather prediction models. *Monthly Weather Review*, *133*, 409–429.

Chelton, D. B., Freilich, M. H., Sienkiewicz, J. M., & Von Ahn, J. M. (2006). On the use of QuikSCAT scatterometer measurements of surface winds for marine weather prediction. *Monthly Weather Review*, *134*, 2055–2071.

Chelton, D. B., Schlax, M. G., Freilich, M. H., & Milliff, R. F. (2004). Satellite measurements reveal persistent small-scale features in ocean winds. *Science*, *303*, 978–983.

Chelton, D. B., & Wentz, F. J. (2005). Global high-resolution satellite observations of sea-surface temperature for numerical weather prediction and climate research. *Bulletin of the American Meteorological Society*, *86*, 1097–1115.

da Silva, A. M., Young, C. C., & Levitus, S. (1994). *Algorithms and procedures. Atlas of Surface Marine Data 1994*, *Vol. 1*. NOAA Atlas NESDIS.

Department of Defense. (2001). *Ehime Maru* Environmental Assessment: Finding Of No Significant Impact. Pearl Harbor: Hawaii. Online at: http://www.smdcen.us/pubdocs/

Freilich, M. H. (1997). Validation of vector magnitude datasets: effects of random component errors. *Journal of Atmospheric and Oceanic Technology*, *14*, 695–703.

Freilich, M. H., & Dunbar, R. S. (1999). The accuracy of the nscat-1 vector winds: comparisons with national data buoy center buoys. *Journal of Geophysical Research*, *104*, 11231–11246.

Freilich, M. H., Long, D. G., & Spencer, M. W. (1994). SeaWinds: a scanning scatterometer for ADEOS II—Science overview. *Proceedings of the international geoscience and remote sensing symposium* (pp. 960–963). Pasadena, California: IEEE.

International Petroleum Industry Environmental Conservation Association. (2000). A Guide to Contingency Planning for Oil Spills on Water. Online at: http://www.ipieca.org/downloads/oil_spill/oilspill_reports/English/Vol2_ContPlanning_1050.71KB.pdf

Jury, M. R., & Walker, N. (1988). Marine boundary layer modification across the edge of the Agulhas Current. *Journal of Geophysical Research*, *93*, 647–654.

Kent, E. C., Challenor, P. G., & Taylor, P. K. (1999). A statistical determination of the random observational errors present in voluntary observing ships meteorological reports. *Journal of Atmospheric and Oceanic Technology*, *16*, 905–914.

Lindzen, R. S., & Nigam, S. (1987). On the role of sea surface temperature gradients in forcing low-level winds and convergence in the Tropics. *Journal of Atmospheric Science*, *44*, 2418–2436.

Mantua, N. J., & Hare, S. R. (2002). The Pacific Decadal Oscillation. *Journal of Oceanography*, *58*(1), 35–44.

Mears, C. A., Smith, D. K., & Wentz, F. J. (2000, July). Detecting rain with QuikSCAT. *International geoscience and remote sensing symposium proceedings.* Honolulu, Hawaii: IEEE.

Mears, C. A., Smith, D. K., & Wentz, F. J. (2001). Comparison of SSM/I and buoy-measured wind speeds from 1987 to 1997. *Journal of Geophysical Research*, *106*, 11719–11729.

Milliff, R. F., Morzel, J., Chelton, D. B., & Freilich, M. H. (2004). Wind stress curl and wind stress divergence biases from rain effects on QSCAT surface wind retrievals. *Journal of Atmospheric and Oceanic Technology*, *21*(8), 1216–1231.

Musial, W., & Butterfield, S. (2004). Future for Offshore Wind Energy in the United States: Preprint; NREL Report No. CP-500-36313. National Renewable Energy Laboratory, Golden, Colorado. Online at: http://www.nrel.gov/docs/fy04osti/36313.pdf

National Climatic Data Center. (2004). Data documentation for dataset 9757 (DSI-9757): U.S. Navy Marine Climatic Atlas. Asheville, North Carolina. Online at: http://www1.ncdc.noaa.gov/pub/data/documentlibrary/tddoc/td9757.pdf

NMOSCP. (2005). Australia's "National Plan to Combat Pollution of the Sea by Oil and Other Noxious and Hazardous Substances" (p. 96). Online at: http://www.amsa.gov.au/Publications/OILPLAN/Oilplan.pdf

O'Neill, L. W., Chelton, D. B., & Esbensen, S. K. (2003). Observations of SST-induced perturbations of the wind stress field over the Southern Ocean on seasonal time scales. *Journal of Climate*, *16*, 2340–2354.

O'Neill, L. W., Chelton, D. B., Esbensen, S. K., & Wentz, F. J. (2005). High-resolution satellite measurements of the atmospheric boundary layer

response to SST variations along the Agulhas Return Current. *Journal of Climate*, *18*, 2706−2723.

Rasmusson, E. M., & Carpenter, T. H. (1982). Variations in tropical sea surface temperature and surface wind fields associated with the Southern Oscillation/El Niño. *Monthly Weather Review*, *110*, 354−384.

Roper, W. (2004). Geospatial Informatics Applications for Disaster Management. 36th Joint Meeting Panel on Wind and Seismic Effects, Washington, District of Columbia. Online at: http://www.pwri.go.jp/eng/ujnr/joint/36/36ag.htm

Samelson, R. M., Skyllingstad, E. D., Chelton, D. B., Esbensen, S. K., O'Neill, L. W., & Thum, N. A. (2006). On the coupling of wind stress and sea surface temperature. *Journal of Climate*, *19*(8), 1557−1566.

Sanderson, W. G., Tiercelin, C., & Villanueva, J. (2001). Accident of the oil tanker "Jessica" off the Galapagos Islands (Ecuador) January 16, 2001: Final Report to European Commission. Online at: http://europa.eu.int/comm/environment/civil/marin/reports_publications/jessica_report.pdf

Schlax, M. G., Chelton, D. B., & Freilich, M. H. (2001). Sampling errors in wind fields constructed from single and tandem scatterometer datasets. *Journal of Atmospheric and Oceanic Technology*, *18*, 1014−1036.

Slutz, R. J., Lubker, S. J., Hiscox, J. D., Woodruff, S. D., Jenne, R. L., Joseph, D. H., et al. (1985). *COADS, Comprehensive Ocean-Atmosphere Data Set, Release 1.* Climate research program Boulder, Colorado: Environmental Research Laboratory.

Small, J. R., Xie, S-P., Wang, Y., Esbensen, S. K., & Vickers, D. (2005). Numerical simulation of boundary layer structure and cross-equatorial flow in the eastern Pacific. *Journal of Atmospheric Science*, *62*, 1812−1830.

Stoffelen, A. (1998). Toward the true near-surface wind speed: error modeling and calibration using triple co-location. *Journal of Geophysical Research*, *103*, 7755−7766.

Sweet, W. R., Fett, R., Kerling, J., & LaViolette, P. (1981). Air–sea interaction effects in the lower troposphere across the north wall of the Gulf Stream. *Monthly Weather Review*, *109*, 1042−1052.

Wallace, J. M., Mitchell, T. P., & Deser, C. (1989). The influence of sea surface temperature on surface wind in the eastern equatorial Pacific: seasonal and interannual variability. *Journal of Climate*, *2*, 1492−1499.

Woodruff, S. D., Slutz, R. J., Jenne, R. L., & Steurer, P. M. (1987). A comprehensive ocean-atmosphere data set. *Bulletin of the American Meteorological Society*, *68*, 1239−1250.

Xie, S.-P. (2004). Satellite observations of cool ocean-atmosphere interaction. *Bulletin of the American Meteorological Society*, *85*, 195−208.